ACS OMEGA

http://pubs.acs.org/journal/acsodf

Article

Study on Evaporation Characteristics of Water in Annular Liquid Pool at Low Pressures

Rui-Feng Guo, Li Zhang, Dong-Ming Mo, Chun-Mei Wu, and You-Rong Li*

Cite This: *ACS Omega* 2021, 6, 5933−5944

Read Online

ACCESS | Metrics & More | Article Recommendations

ABSTRACT: In order to investigate the energy transfer mechanism and the nonequilibrium effect during water evaporation in its own pure vapor at low pressures, a series of precise measurements are conducted to obtain the temperature profile near the liquid−vapor interface and the evaporation rates in an annular pool in a closed chamber. The results show that the interface temperature of the vapor side is higher than that of the liquid side when water evaporates in its own pure vapor at low pressures (ranging from 394 to 1467 Pa), the temperature discontinuity across the interface exists in all experimental conditions. The magnitude of the temperature discontinuity is strongly affected by the vapor pressure. A uniform temperature layer with a thickness of about 2 mm is found below the evaporating interface because of the coupling effect of evaporation cooling and thermocapillary convection. The energy required for evaporation is mainly transferred by thermocapillary convection in the uniform temperature layer. Furthermore, the numerical simulation results confirm that the evaporation flux near the cylinders is much larger than that at the middle region, which implies that most of the latent heat required for evaporation is transferred to the interface near the cylinders.

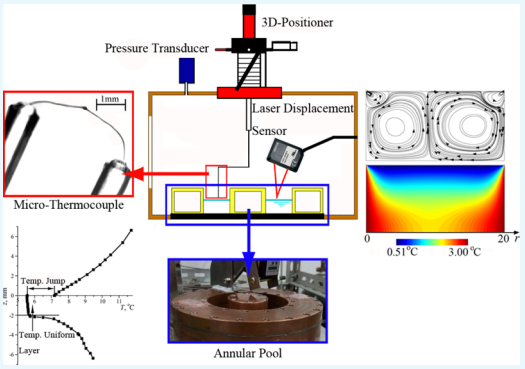

INTRODUCTION

The evaporation process is very important for chemistry, medicine, agriculture, biology, engineering and so forth.[1−3] Although many investigations have been carried out, the mechanism of the phase change is still not fully understood because of the hydrodynamic effects in the bulk liquid phase and the nonequilibrium effect at the liquid−vapor interface.

From a microperspective, molecules pass through the liquid−vapor interface from the liquid phase to vapor phase when the evaporation happens, which is a typical nonequilibrium process including temperature discontinuity and mass transfer. Hertz[4] and Knudsen[5] proposed a classical kinetic theory of gases (KTG) to model the evaporation process. This theory is still widely used today. In KTG, these nonequilibrium processes are considered to be occurring in the Knudsen layer that is a vapor layer with a thickness of the order of molecular mean free path near the liquid−vapor interface. The temperature discontinuity exists across the liquid−vapor interface, which is one of the important driving forces of evaporation process. However, in many research studies, the temperature profile at the evaporating interface is assumed to be continuous,[6,7] which will inevitably lead to a difference from the actual energy transfer process, especially at low pressures.

The temperature discontinuity at liquid−vapor interface during evaporation has been known for a long time[8,9] in theory. In the experimental studies, Shankar and Deshpande[10] made the first attempt to measure the temperature discontinuity at the liquid−vapor interface using ten thermocouples with a diameter of 300 μm. They confirmed the existence of the temperature discontinuity and found that the temperature discontinuity on the mercury surface is larger than those on the water and Freon 113 surfaces. However, the location of the liquid−vapor interface was not precisely determined in their temperature measurements. Fang and Ward[11] measured the temperature profile near the interface with a thermocouple with a diameter of 25 μm. They found that the temperature of the vapor side is higher than that of the liquid side and the maximum temperature discontinuity reaches 7.8 K. However, both the magnitude and the direction of the temperature discontinuity do not accord with those described by the kinetic theory. Some further experiments[12−16] were carried out and a new expression for the evaporation rate based on the statistical rate theory was proposed.[16,17] Bond and Struchtrup[18] used the kinetic theory to simulate the evaporation process and calculate the temperature disconti-

Received: January 8, 2021
Accepted: February 12, 2021
Published: February 19, 2021

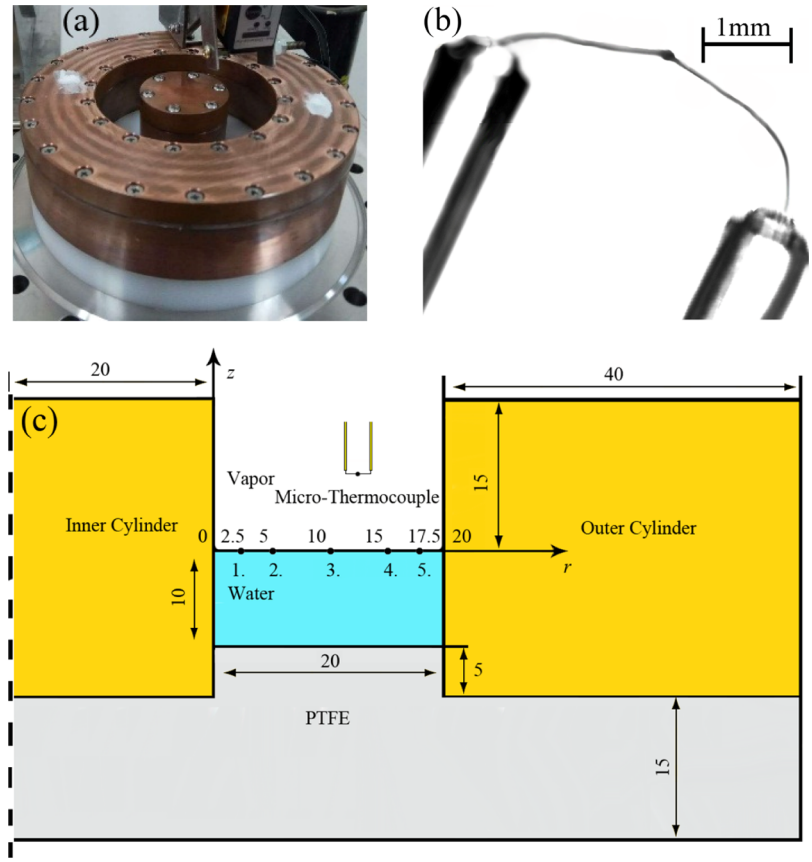

Figure 1. Annular pool (a), microthermocouple (b), and detail position (c) of temperature measurement points from points 1 to 5 (unit: mm).

nuity. It was found that the magnitude of temperature discontinuity depends strongly on the heat flux on the vapor side near the evaporating interface. In 2007, Badam et al.[19] carried out a series of experiments with vapor heating in an evaporation chamber to form steep temperature gradients on the vapor side of the interface. It was found that the direction of the temperature discontinuity is the same as the experimental results of Ward et al.[11−16] However, the magnitude of the temperature discontinuity is very large and the maximum temperature discontinuity achieves 27.83 K, they believed that the heat flux on the vapor side has a great influence on the temperature discontinuity. In addition, other similar temperature distributions at a low pressure were also obtained by the experiments.[20,21]

The experimental results in low-pressure evaporating chambers showed that the temperature of the vapor side is higher than that of the liquid side, but some investigations at atmosphere conditions gave different conclusions. Zhu and Liu[22] measured the temperature discontinuity in a shallow planar liquid layer in an atmosphere with a 50 μm thermocouple, and a horizontal temperature difference was imposed to produce thermocapillary convection. It was found that the direction of temperature discontinuity eventually changes with the increase of the temperature difference. Gatapova et al.[23,24] measured the temperature profile across the liquid−gas interface by a special thermocouple with a 4 μm bead size in an atmosphere. The thin liquid layer is heated from the bottom. When the heater temperature is low, the temperature on the gas side is higher than that on the liquid side. With the increase of the heating power, the interface temperature difference between the gas side and the liquid side decreases, and the temperature on the liquid side is finally higher than that on the gas side.

On the other hand, Hołyst and Litniewski[25] used molecular dynamics simulation (MDS) to investigate the Lennard-Jones fluid evaporation process. It was found that the temperature is continuous when the density ratio of the liquid to the vapor is small enough, but the temperature discontinuity appears when the density ratio is more than 10. Obviously, the density ratio is much greater than 10 for water evaporation at low pressures, so the temperature discontinuity can be detected according to their conclusions. In the previous experiments, the magnitude and the direction of the temperature discontinuity are affected by many macrofactors, including thermocapillary flow, buoyancy convection, heating mode, and so forth. However, MDS cannot give a more detail description on the effects of these factors on the temperature discontinuity.

Furthermore, the uniform temperature layer below the evaporating interface has been found in the temperature measurements.[26−29] The uniform temperature layer is believed to be related to thermocapillary convection and has a large effect on the energy transfer mode in the liquid layer. Moreover, buoyancy convection may also influence the temperature distribution and uniform temperature layer in the liquid phase.[20] In fact, because of different heating modes and evaporation environments, the mechanisms of energy transfer are different. Therefore, the direction and magnitude of the temperature discontinuity have a large difference in the reported results.

In previous studies, most of the experimental devices were heated from their bottom or in the vapor phase, and there was only one fixed measurement point on the free surface of the

https://dx.doi.org/10.1021/acsomega.1c00134
ACS Omega 2021, 6, 5933−5944

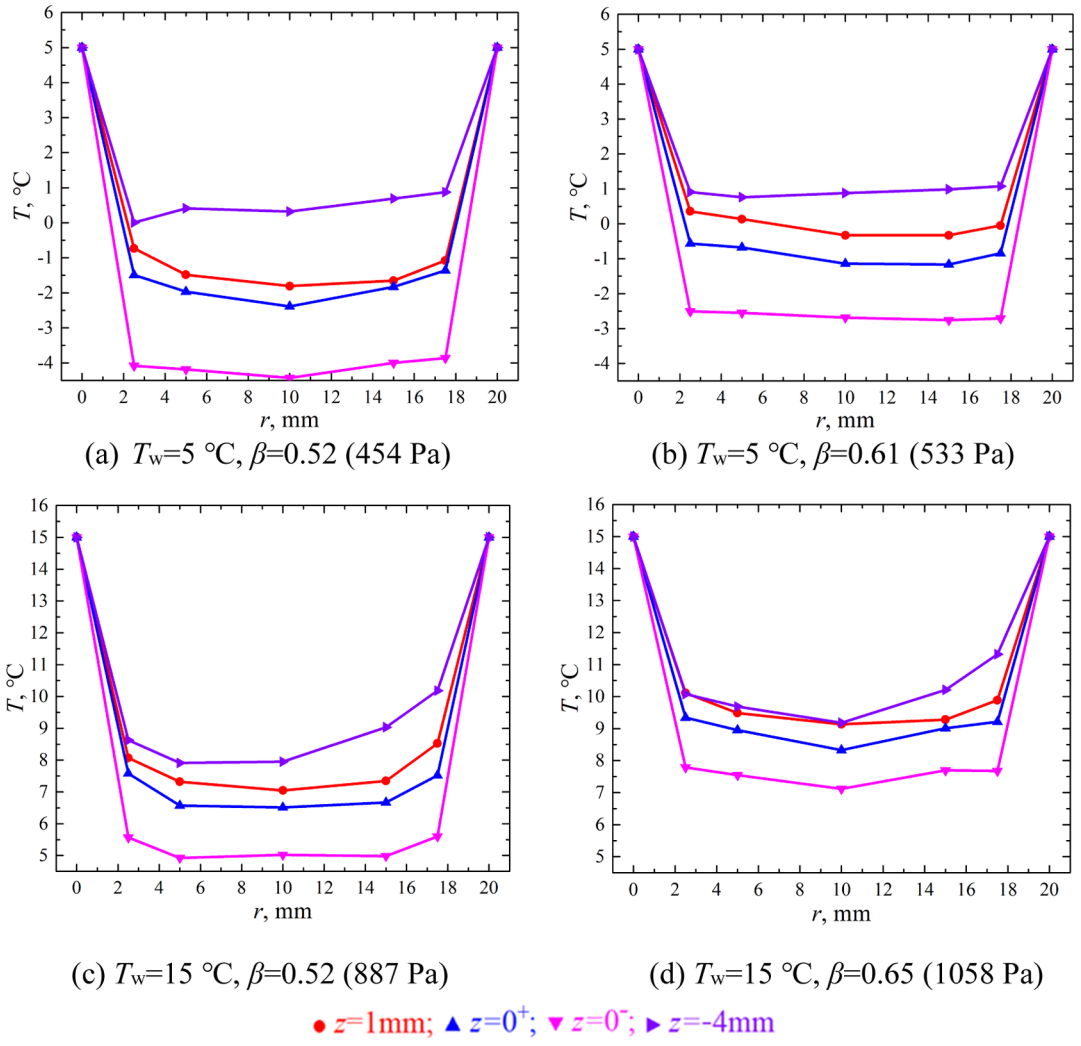

Figure 2. Radial temperature distribution near the liquid−vapor interface. $z > 0$ is the vapor phase and $z < 0$ is the liquid phase.

liquid layer so that no comparison between different measurement points can be conducted. Therefore, the mechanism of energy transfer in the liquid layer was difficult to be revealed. In the present experiments, water is heated by the inner and outer cylinders of the annular pool and the bottom can be considered adiabatic. The temperature distribution and energy transfer mode are quite different from those in the previous studies. By measuring the temperatures at different measurement points in the radial direction, the distribution of temperature discontinuity in the radial direction is determined, and the relationship between evaporation rate and temperature discontinuity is further analyzed. Then, combined with the experimental and numerical simulation results, the energy transfer mechanism can be summarized.

RESULTS AND DISCUSSION

Temperature Distribution near the Interface. In order to obtain the temperature profile near the interface in the annular pool (see Figure 1a), a T-type microthermocouple (see Figure 1b) is used in the temperature measurement. The detailed location of the measurement points is shown in Figure 1c. In the experiments, the working fluid is cold water. Its temperature can be decreased to 253 K when the steady evaporation in the vapor happens.[12] Considering the evaporative cooling effect on the liquid−vapor interface, the cylinder temperature T_w is maintained at (3−15) °C in order to study the temperature discontinuity and energy transfer mode in different cylinder temperatures. Moreover, the pressure ratio β is introduced to indicate the relative magnitude of the pressure in experiments, which is defined as the ratio of the vapor pressure P^v to the saturation pressure of water at the cylinder temperature T_w

$$\beta = \frac{P^v}{P_{sat}(T_w)} \tag{1}$$

The radial temperature distributions near the liquid−vapor interface are shown in Figure 2, where $z = 0^+$ and $z = 0^-$ correspond, respectively, to the interface temperatures of the vapor side and the liquid side. On the liquid side, because of the existence of the large radial temperature gradient on the free surface near the cylinders, the thermocapillary flows from the cylinders to the middle of the free surface will be induced, the radial temperature variation is not obvious at a low cylinder temperature.

The typical axial temperature distribution near the liquid−vapor interface is shown in Figure 3. In the vapor phase, the temperature rises almost linearly with the increase of the distance from the interface that means the heat conduction is a

https://dx.doi.org/10.1021/acsomega.1c00134
ACS Omega 2021, 6, 5933−5944

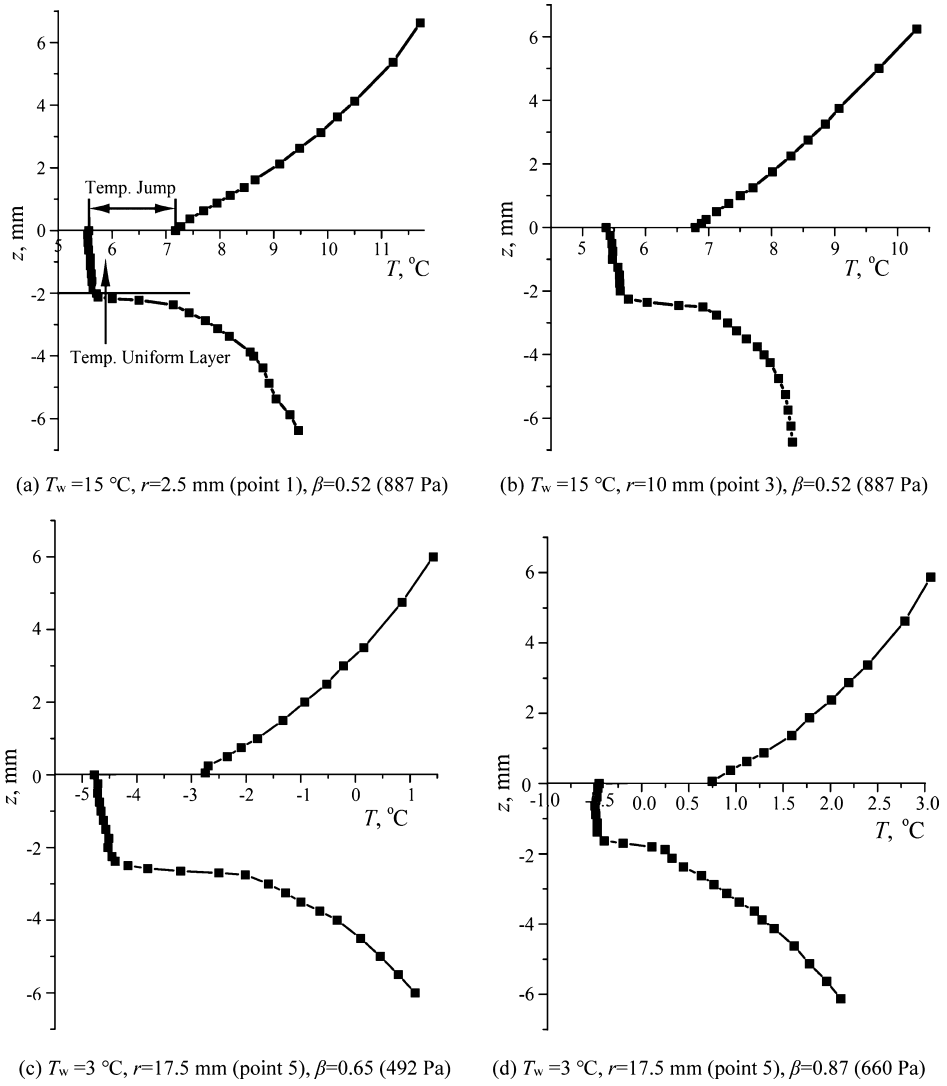

(a) T_w =15 °C, r=2.5 mm (point 1), β=0.52 (887 Pa) (b) T_w =15 °C, r=10 mm (point 3), β=0.52 (887 Pa)

(c) T_w =3 °C, r=17.5 mm (point 5), β=0.65 (492 Pa) (d) T_w =3 °C, r=17.5 mm (point 5), β=0.87 (660 Pa)

Figure 3. Typical axial distribution of the temperature near the liquid−vapor interface.

dominant mode for the heat transport. While in the liquid phase, the axial temperature variation near the liquid−vapor interface is small. This layer with a small axial temperature gradient is called the uniform temperature layer,[26] which is considered to be related to the mixing process of the thermocapillary flow near the evaporating interface. In the temperature measurements, the thickness of the uniform temperature layer ranges from 1 to 2.5 mm, which is larger than the results in refs[26,28] because of the large scale of the liquid layer and the different heating modes. Below the uniform temperature layer, the temperature rises rapidly and nonlinearly, especially at the measurement points close to the cylinders. That means strong heat conduction and appreciably buoyancy convection exist below the uniform temperature layer. More energy is transferred to the uniform temperature layer by heat conduction and buoyancy convection near the cylinders than that away from the cylinders. The conductive heat flux from the liquid phase below the uniform temperature layer and from the vapor phase can be calculated by the Fourier law

$$q_c = -k\frac{\partial T}{\partial z} \quad (2)$$

The typical radial distribution of the conductive heat fluxes in two phases is shown in Figure 4. The energy transferred to the uniform temperature layer by heat conduction and buoyancy convection in the liquid phase is much greater than that transferred to the interface by heat conduction from vapor. When T_w = 10 °C and β = 0.65, the heat fluxes in the liquid phase at points 1 and 5 are much higher than those at other points. It hints that the buoyancy convection plays an important role in energy transfer in the liquid phase.

The average evaporation heat flux on the liquid−vapor interface can be estimated by $\overline{h^{lv}}\overline{j^{LV}}$, $\overline{h^{lv}}$ is the average enthalpy difference at the five measurement points and $\overline{j^{LV}}$ is the average evaporation mass rate calculated from a laser displacement sensor. The average evaporation heat fluxes corresponding to Figure 4 are, respectively, 3078 and 5963 W/m^2, which are much higher than the conductive heat fluxes from the liquid phase below the uniform temperature layer. That means the latent heat required for evaporation at the interface is mainly provided by thermocapillary convection, while the buoyancy convection and heat conduction provide a small amount of the evaporation latent heat.

Liquid−Vapor Interface Temperature Discontinuity. According to the axial temperature distribution obtained in the

https://dx.doi.org/10.1021/acsomega.1c00134
ACS Omega 2021, 6, 5933−5944

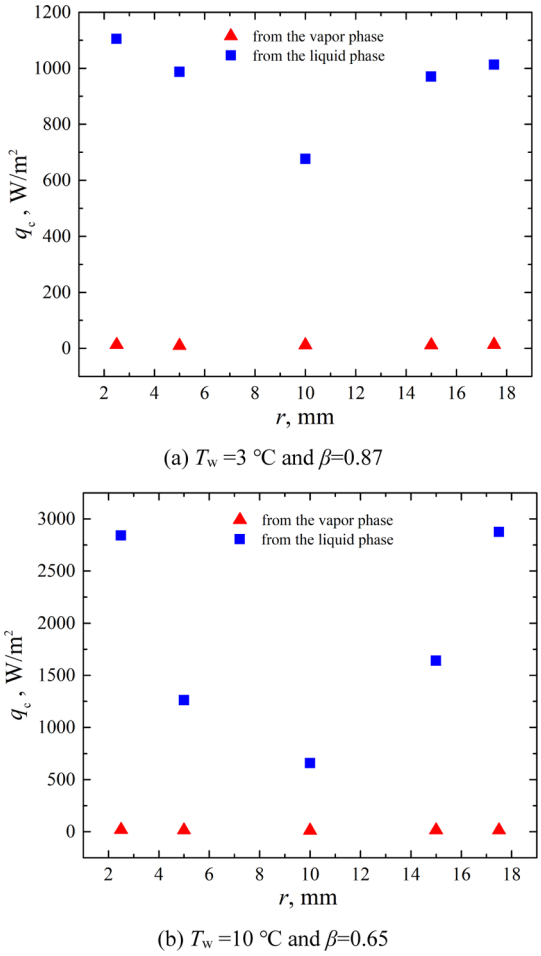

Figure 4. Typical radial distribution of the conductive heat fluxes from two phases.

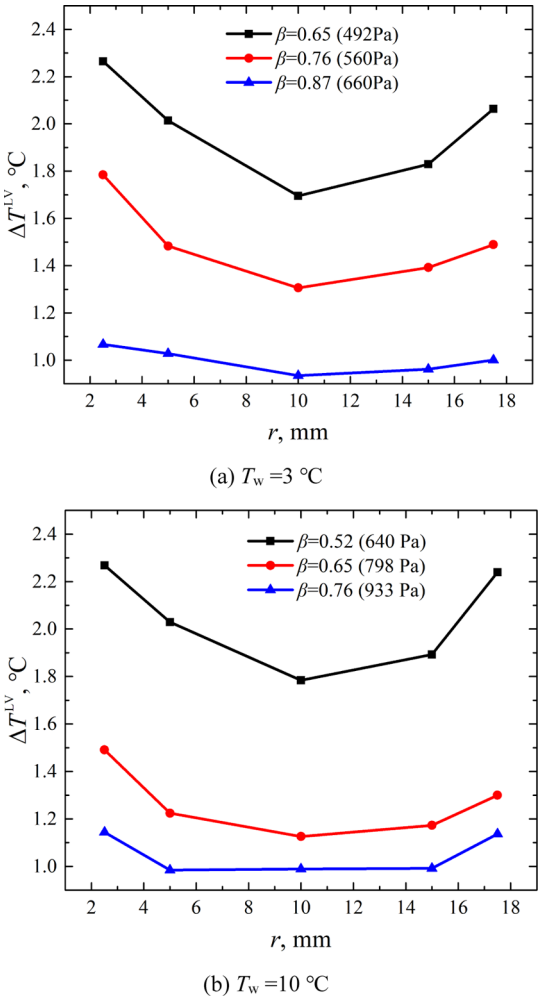

Figure 5. Radial distribution of interface temperature discontinuities at different cylinder temperatures.

measurements, the temperature discontinuities across the liquid−vapor interface exist under all experimental conditions and the interface temperature of the vapor side is higher than that of the liquid side. The typical radial distributions of interface temperature discontinuities are shown in Figure 5. Most of the temperature discontinuities across the interface measured in the experiments range from 1 to 2 °C. It can be observed clearly that the temperature discontinuity increases with the decrease of the pressure ratio. In addition, the temperature discontinuities measured at the points close to the cylinders (points 1 and 5) are larger than those at other points.

The evaporation process is a nonequilibrium thermodynamic process. Therefore, the higher the evaporation rate is, the farther the evaporation process deviates from the equilibrium state. Because of the higher surface temperature near the cylinders, the local evaporation rate is larger, the temperature discontinuity near the cylinders is higher than that in the middle region. With the decrease of the vapor pressure, the local evaporation rate increases, so the temperature discontinuity at all points increases. On the other hand, as it is discussed in previous research studies,[18−20] the heat flux from the vapor may have an influence on the magnitude of the temperature discontinuity. With the increase of the heat flux from vapor, the temperature discontinuity increases. However, to study the influence of the thermocouple on temperature jump measurement, Kazemi et al.[30] simulated the temperature measurement process of the thermocouple near the interface. They found that the heat conduction through the thermocouple wires can cause a large temperature measurement error in the vapor phase. Jafari et al.[31] obtained the same conclusion through Direct Simulation Monte Carlo Method. Therefore, the temperature discontinuity should be measured under a low heat flux from the vapor side.

Figure 6 shows the relationship between the conductive heat flux from the vapor and temperature discontinuity obtained from experiments, which can be expressed as

$$\Delta T^{LV} = 0.098 q_{c,v} + 0.296 \quad (3)$$

It is obvious that with the increase of the heat flux from the vapor, the temperature discontinuity tends to increase linearly, which means that the conductive heat flux from the vapor has an important effect on temperature discontinuity.

In this work, the direction of the temperature discontinuity stays the same. The reasonable explanation is that the high energy molecules can preferentially be across the liquid−vapor interface from the liquid phase to vapor phase, so the vapor temperature is higher than the liquid temperature on the free surface. The relationship between the temperature discontinuity and the cylinder temperature is shown in Figure 7. It is clear that the temperature discontinuity tends to decrease with the increase of the cylinder temperature at the same pressure ratio. According to the temperature profile, as the cylinder

https://dx.doi.org/10.1021/acsomega.1c00134
ACS Omega 2021, 6, 5933−5944

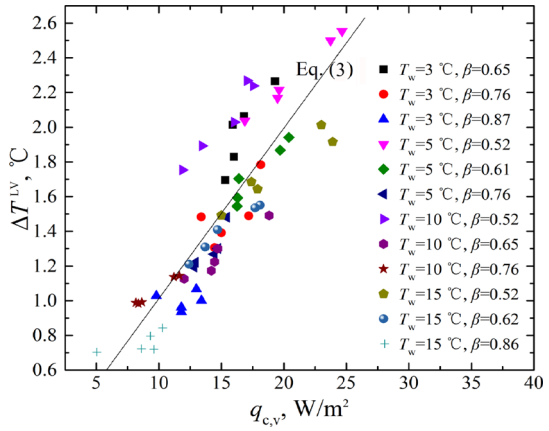

Figure 6. Relationship between the interface temperature discontinuity and the heat flux from the vapor side.

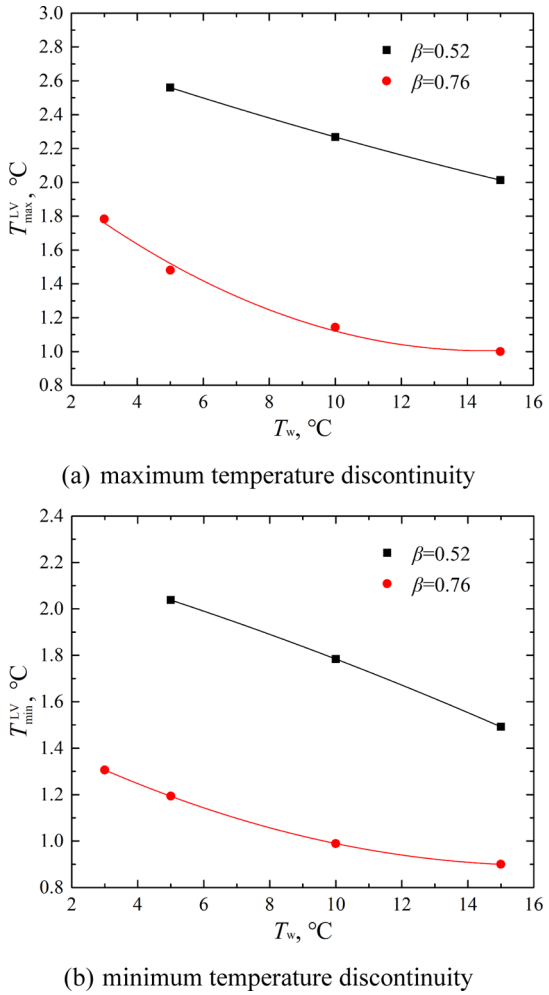

Figure 7. Effect of the cylinder temperature on the temperature discontinuity.

temperature increases, the surface temperature also increases, the heat flux from the vapor side decreases (see Figure 7). On the other hand, when the cylinder temperature is low, due to evaporative cooling effect, the temperature in most regions of the liquid phase is lower than 4 °C. The lighter fluid exists near the surface, while the denser fluid appears near the bottom in the liquid phase. In this case, buoyancy convection is very weak. When the cylinder temperature is high, the denser fluid exists near the interface while the lighter fluid appears near the bottom in the liquid phase, therefore, the buoyancy convection is likely to be induced. With the increase of the cylinder temperature, the buoyancy convection in the liquid phase becomes stronger, and more energy is transferred to the interface. The heat flux from the vapor by conduction is reduced. That may be the reason that the interface temperature discontinuity decreases with the increase of the cylinder temperature.

Uniform Temperature Layer. From the axial temperature distribution, a uniform temperature layer exists below the liquid−vapor interface. This phenomenon has been found in previous temperature measurement experiments, especially at low vapor pressures, which will change the energy transfer mode in the liquid layer. Considering the evaporation cooling effect at the liquid−vapor interface, the temperature near the cylinders is much higher than the temperature in the middle region on the free surface. The radial temperature gradient will drive the fluid to flow from the cylinders to the middle region along the free surface, and the backflows to the cylinders appear below the free surface. During this process, the fluid near the interface is fully mixed and the uniform temperature layer appears.

In 2001, Ward and Stanga[26] found a uniform temperature layer both in evaporation and condensation, and the thickness is about 0.5 mm. In their research studies, thermocapillary convection at the liquid−vapor interface is considered to be the reasonable explanation. To investigate the mechanism of the uniform temperature layer, Ward and Duan[27] used a cantilevered probe to measure the flow below the evaporating interface and further confirmed the existence of thermocapillary convection. Moreover, Song and Nobes[32] investigated the thermocapillary convection induced by evaporation at low pressures by using particle image velocimetry, the regions with a relatively uniform temperature appear below the free surface near the sidewalls of the cuvette, the positions coincide with that of the thermocapillary flow cells. Thus, the thermocapillary flow should be the reason for the uniform temperature layer.

According to the temperature profile in the liquid phase, the thickness δ of the uniform temperature layer can be determined. Figure 8 shows the variation of the thickness of the uniform temperature layer in the radial direction. Obviously, the thicknesses measured at points 1 and 5 are larger than those at other points, which means that the mixing process is more intense at points 1 and 5 than that at other points. In addition, a sharp variation of the surface temperature in the radial direction will result in the minimum thickness of the uniform temperature layer near the cylinders.

On the condition of the low cylinder temperature, there is almost no buoyancy convection in the liquid phase. With the decrease of the pressure ratio, the thickness of the temperature uniform layer tends to increase, as shown in Figure 8a. When the cylinder temperature is high, the thickness of the layer is affected by pressure ratio and buoyancy convection. For example, when T_w = 15 °C, with the decrease of the pressure ratio, the buoyancy convection is enhanced, the thickness of the uniform layer increases rapidly (see Figure 8b).

Numerical Simulation. In order to further analyze the energy transfer mechanism, a steady-state model is used to simulate the evaporation process in the annular liquid pool at

https://dx.doi.org/10.1021/acsomega.1c00134
ACS Omega 2021, 6, 5933−5944

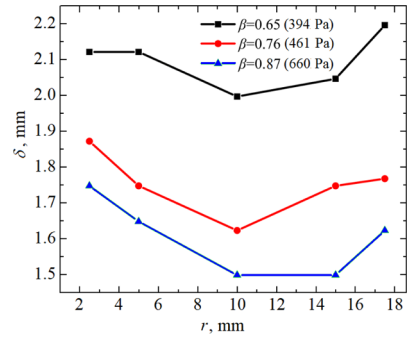

(a) T_w =3 ℃

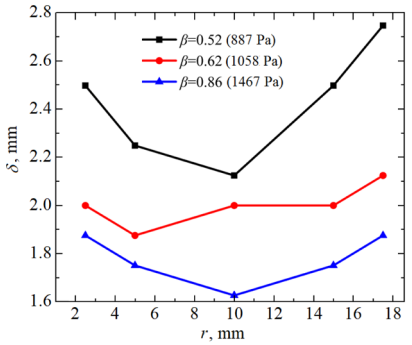

(b) T_w =15 ℃

Figure 8. Effect of the pressure ratio on the thickness of the uniform temperature layer.

low pressures. The liquid phase, vapor phase, and the evaporating interface are included in the two-sided model.

Both the liquid and vapor phases can be considered incompressible. At the liquid−vapor interface, the absolute pressure is set as the vapor pressure measured by the pressure transducer in the experiments, the interface temperature discontinuity $\Delta T^{LV} = T_I^V - T_I^L$ is the average temperature discontinuity at five points in the temperature measurements. The evaporation flux can be calculated by KTG and the thermocapillary force is considered on the evaporating interface.

The typical flow field and temperature distribution in the vapor phase are, respectively, as shown in Figure 9a,b, the radial distribution of evaporation flux is presented in Figure 9c. The numerical results show that the evaporation flux near the cylinders is much larger than that at the middle region of the evaporating interface. It means most of the energy required for evaporation in the liquid pool is transferred to the evaporating interface near the cylinders. A comparison of the average evaporation rates $\overline{j^{LV}}$ obtained from experiments and simulation is presented in Figure 9d. Both the experimental and simulation results show that the average evaporation flux increases with the decrease of vapor pressure. Moreover, it is worth noting that the evaporation rate increases significantly with the decrease of the pressure ratio when the cylinder temperature is 15 °C, the reason is that the buoyancy convection greatly promotes the evaporation process. When the cylinder temperature is low, the liquid temperature near the interface will be lower than 4 °C with the decrease of the pressure ratio. In this case, the buoyancy convection is suppressed.

The flow and thermal fields in the liquid phase under different pressure ratios at T_w = 3 °C are shown in Figure 10. Obviously, there are two thermocapillary cells near the

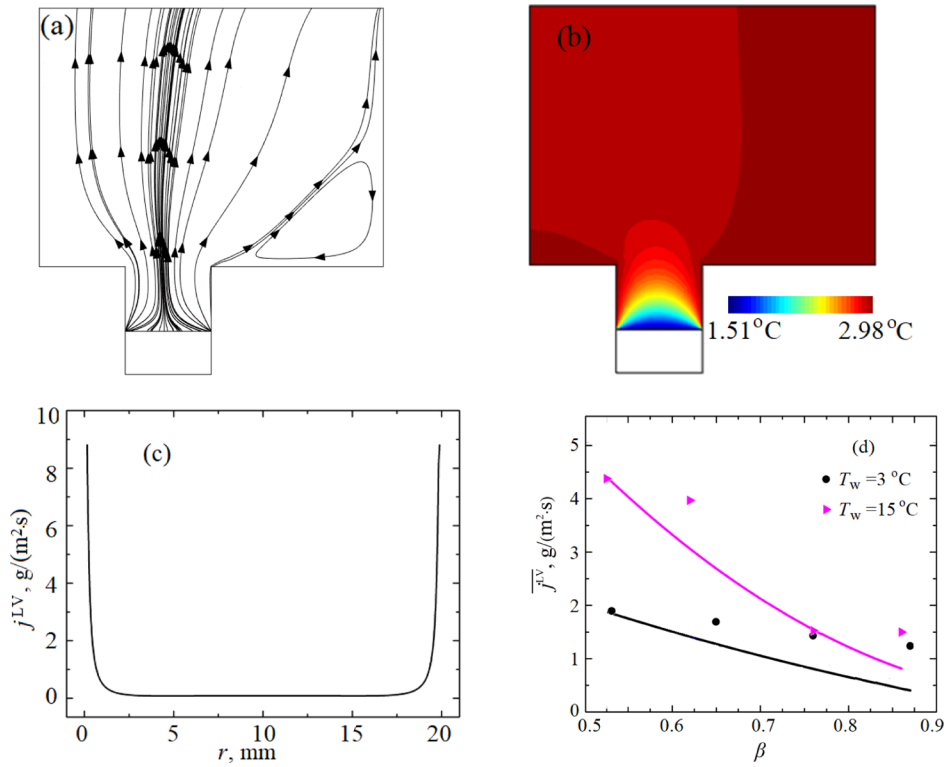

Figure 9. Flow field of the vapor phase (a), temperature distribution of the vapor phase (b), and radial distribution of the evaporation flux (c) at T_w = 3 °C and β = 0.87. The comparison of the average evaporation rates between experimental (points) and simulation (solid line) results (d).

https://dx.doi.org/10.1021/acsomega.1c00134
ACS Omega 2021, 6, 5933−5944

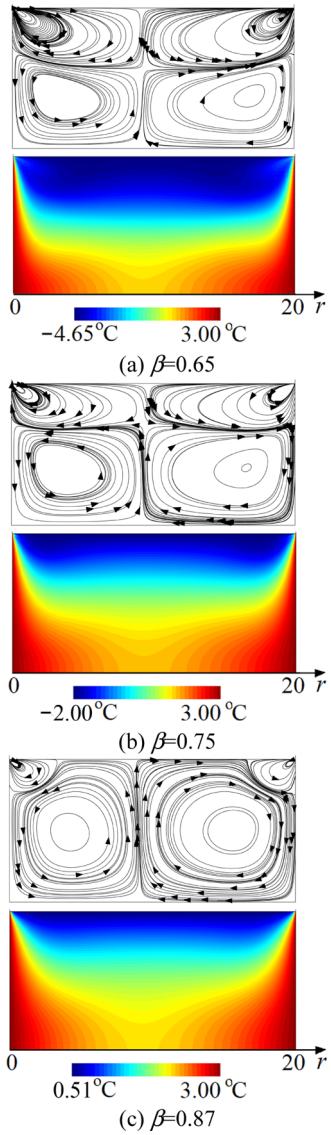

Figure 10. Flow (upper) and thermal (low) fields in the liquid phase at T_w = 3 °C.

evaporating interface because of the radial temperature gradient near the cylinders. Moreover, two buoyancy driven cells can also be observed below the thermocapillary vortexes. Furthermore, the flow cells near the outer cylinder are stronger than those near the inner cylinder. With the decrease of the pressure ratio, the radial temperature gradient on the free surface near the cylinders increases, the thermocapillary cells are enhanced, while the buoyancy driven vortexes tend to become smaller because of the suppressing effect of the thermocapillary cells.

The comparison of the interface temperatures of the liquid side between the simulation results and experimental measurements is shown in Figure 11a. As the pressure ratio decreases, both the simulation and experimental results indicate that the interface temperature of the liquid side drops because of the evaporation cooling effect. The simulated curve has a good agreement with the experimental data, the maximum difference is about 0.5 °C. Figure 11b,c shows the comparison of the axial temperature distributions. In the liquid phase, the uniform temperature layer can be seen in the simulated axial temperature distribution and the thickness of the uniform temperature layer is close to the experimental value (about 2 mm). While in the vapor phase, the axial temperature distributions obtained by the experiment and simulation are basically consistent. In the simulation, the liquid−vapor interface temperature discontinuity is set as the average temperature discontinuity at five points in the experiments, so there is a deviation between the experimental and simulated temperature distributions.

CONCLUSIONS

A series of experimental measurements and numerical simulations are conducted for water evaporation processes in its own pure vapor at low pressures. According to the experiment and simulation results, the following conclusions can be drawn. When water evaporates in its own pure vapor at low pressures, the evaporating interface temperature of the vapor side is higher than that of the liquid side according to the temperature measurement results, so there is an interface temperature discontinuity. The interface temperature discontinuity increases obviously with the decrease of the pressure ratio. Moreover, the heat flux from the vapor side has an important effect on the magnitude of the interface temperature discontinuity. A uniform temperature layer exists in the liquid phase near the evaporating interface, which plays an important role for energy transfer in the evaporation. The thickness of the uniform temperature layer increases with the decrease of pressure ratio. The energy is mainly transferred by convection in the uniform temperature layer, while the heat conduction and buoyancy convection are dominant below the uniform temperature layer. The evaporation flux near the cylinders on the free surface is much higher than that in the middle region. Most of the energy required for evaporation in the annular liquid pool is transferred to the interface near the cylinders. At a high cylinder temperature, the buoyancy convection can promote evaporation obviously.

EXPERIMENTAL METHOD

Experimental Apparatus. The scheme of the experimental setup is shown in Figure 12, the annular liquid pool is mounted in a closed stainless-steel chamber. The thickness of the chamber wall is 10 mm. Because of the strong evaporative cooling effect at the evaporating interface at a low vapor pressure, the temperature of liquid and vapor phases near the interface in the closed chamber is lower than that of the atmosphere temperature. The heat flux from the atmosphere can affect the temperature distributions obtained in the temperature measurements. In order to minimize the heat exchange between the chamber and atmosphere, the chamber surface is covered by an insulating layer with a thickness of 25 mm [the thermal conductivity is 0.02 W/(m·K)].

The closed chamber is evacuated by a mechanical vacuum pump to maintain vacuum and eliminate the impurities in the chamber, a metering valve is used to control the pumping rate of the vacuum pump. The vapor pressure in the chamber is measured by a pressure transducer (INFICON, CDG025D, 375-002, which provides highly reliable measurements within the range of 13.3 to 1.33 × 10^5 Pa) mounted at the top of the chamber. The approximate distance between the transducer and the evaporating interface in the annular pool is 100 mm. The pressure in the chamber can be decreased to less than 40 Pa when the mechanical vacuum pump runs for about half an hour.

https://dx.doi.org/10.1021/acsomega.1c00134
ACS Omega 2021, 6, 5933−5944

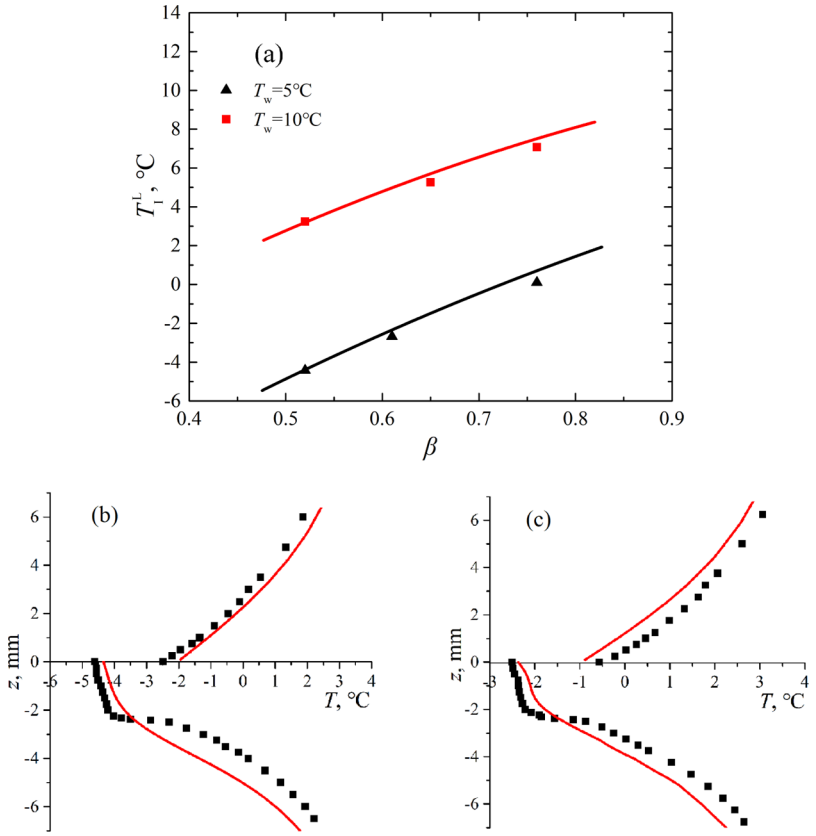

Figure 11. Comparison between experimental measurements (points) and numerical simulations (solid lines). (a) Variation of the interface temperature with the pressure ratio at T_w = 5 °C and T_w = 10 °C. (b) Axial temperature distribution at T_w = 5 °C, r = 5 mm and β = 0.52. (c) Axial temperature distribution at T_w = 5 °C, r = 15 mm and β = 0.61.

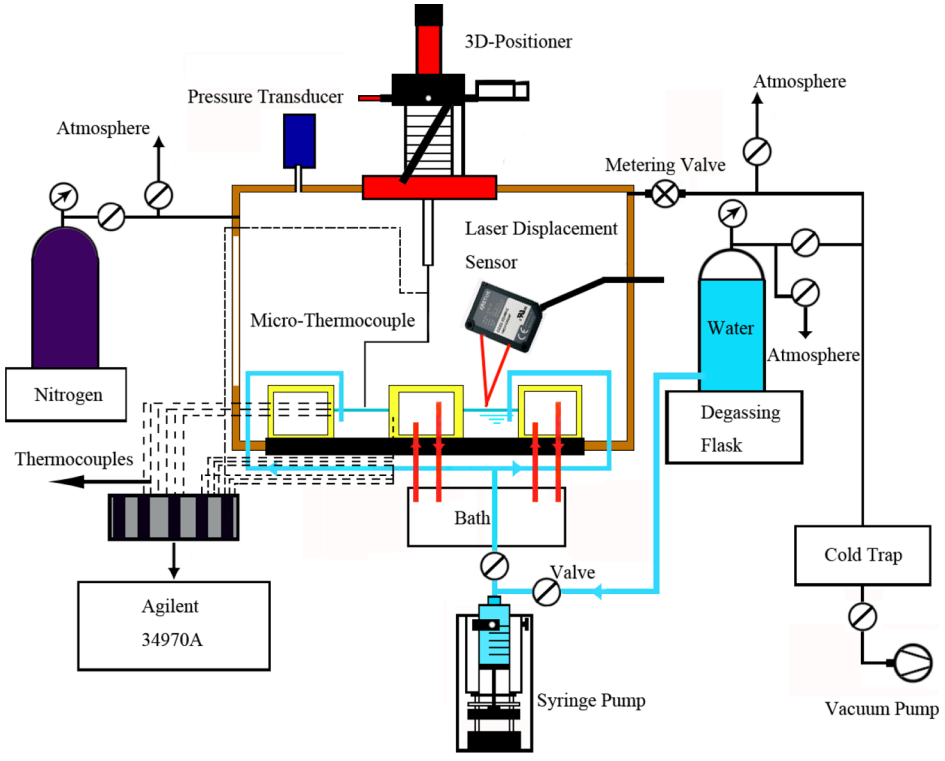

Figure 12. Schematic of the experiment apparatus.

The inner and outer diameters of the annular pool are, respectively, 40 and 80 mm, and the depth is 25 mm. The bottom and cylinders of the annular pool are, respectively, made by PTFE with a thermal conductivity of 0.25 W/(m·K)

https://dx.doi.org/10.1021/acsomega.1c00134
ACS Omega 2021, 6, 5933−5944

and copper with a thermal conductivity of 400 W/(m·K). The flow channels are designed in the inner and outer cylinders of the annular pool to maintain the cylinder temperatures through two thermostatic water baths. In order to obtain the temperature of the cylindrical walls in real time, twelve T-type thermocouples with a diameter of 127 μm are, respectively, embedded into the inner and outer cylinders through the holes with a diameter of 1 mm. The holes are evenly distributed along the circumference and the center of the holes is about 1.5 mm away from the cylindrical walls. Moreover, the junctions of these thermocouples are vertically located 2, 6, and 10 mm above the bottom of the liquid pool. All holes are filled with conductive silica gel to reduce the temperature measurement error. The T-type microthermocouple with a wire diameter of 50 μm used for temperature measurement near the interface is fixed on a three-dimensional (3D) positioner (EMC-B450C-T275TM-1.87-4/MM, Thermionics Northwest, Inc) in the chamber with a resolution of 1 μm in the axial direction (vertically to the liquid−vapor interface) and 10 μm in other two directions.

The position of the liquid−vapor interface and the bottom of the annular pool is measured by a laser displacement sensor (OPTEX CD33) fixed on the outer cylinder of the annular pool. Therefore, the depth of the liquid layer can be determined by the relative position of the liquid−vapor interface and the bottom of liquid pool in real time. The measurement range of a laser displacement sensor is ±5 mm.

Measurement Procedure. After being degassed for more than 5 h in the degassing flask, the distilled water enters into a syringe pump without contacting with the atmosphere. At the same time, the vacuum pump continues to evacuate the closed chamber and the syringe. During this process, a part of the water enters into the annular pool through the supplementary channels and is evaporated totally after about 1 h, so that the chamber is dry. Thereafter, the syringe pumps water into the annular pool to a certain depth (about 13 mm). Before entering the chamber, the water and the cold liquid from a thermostatic water bath exchange heat with each other sufficiently to avoid disturbing the temperature distribution in the annular pool. The vapor pressure in the chamber can be controlled at a fixed value by the metering valve. When the vapor pressure in the chamber is maintained at the predetermined pressure for more than 15 min and the readings of the microthermocouple remains stable, the steady-state evaporation could be considered to have been achieved.

When the depth of water is reduced to 10 mm, the experiment begins. At the beginning of the measurements, the position of the measurement point is determined at z = 8 mm, that is, 8 mm above the liquid−vapor interface. Then, the microthermocouple is moved down slowly and across the interface to the liquid phase by moving a 3D-positioner. The microthermocouple is finally moved to z = −7 mm far from the interface, that is, 7 mm below the interface, the temperature measurement is finished. The temperature discontinuity can be calculated based on the interface temperatures of the liquid side and vapor side. Under the conditions of the same cylinder temperature and pressure ratio, the radial distribution profile near the liquid−vapor interface can be obtained by the axial temperature distribution at different radial positions. Moreover, the depth of the water is recorded in real time by the laser displacement sensor during the temperature measurements, so the average evaporation rate can be calculated by the variation of water depth with time. In the annular liquid pool, the liquid−vapor interface is almost flat, and the meniscus only exists near the cylinders, so the influence of the meniscus can be ignored.

Experimental Uncertainly Analysis. For the vapor pressure measured by a pressure transducer, the precision is 0.2% of reading. The vapor pressure is always lower than 1500 Pa (range from 394 to 1467 Pa) in the experiments, so the error is less than ±3 Pa. This error is not enough to affect the evaporation flux at the liquid−vapor interface. Therefore, the vapor pressure in the chamber can be precisely controlled.

The accuracy of the temperature measurement is particularly important to determine the energy transfer mechanism in two phases and the temperature discontinuity across the liquid−vapor interface. For this purpose, a series of methods are used to reduce the temperature measurement error. The microthermocouple wire is wrapped in the insulation material to minimize the heat exchange with the outside. In order to avoid heat conduction along the wire, the microthermocouple is fashioned into a U shape when it is fixed on the 3D-positioner, as shown in Figure 1b. The ratio of the horizontal length (4 mm) of the U shape to the diameter (50 μm) of the thermocouple is designed to be large enough, so the thermal conduction along the wire can be neglected.[13] Moreover, the junction of the microthermocouple should be as close as possible to the liquid−vapor interface because of the large temperature change near the evaporating interface at low pressures. When the junction reaches approximately 0.5 mm above the interface, the step distance of the 3D-positioner is set as 10 μm for a more precise measurement near the interface. In this case, the nearest distance from the center of the junction to the interface is less than 60 μm. According to the temperature profile measured in the experiments, the maximum temperature gradient from the vapor is about 1.512 °C/mm, so the maximum interface temperature error on the vapor side is 0.09 °C. The influence of the thermocouple diameter on the magnitude of the temperature discontinuity can be ignored. On the other hand, the mean free path of the vapor molecule in the range of experimental pressures varies from 3.80 to 13.61 μm. Therefore, considering the thickness of the Knudsen layer is several mean free paths and the relatively low temperature gradient on the vapor, it can be considered that the temperature measured by the microthermocouple is close enough to the interface temperature of the vapor side. The mean free path λ is calculated by the following equation[33]

$$\lambda = \frac{k_b T^v}{\sqrt{2} P^v \pi d^2} \tag{4}$$

After the temperature measurement is completed, the average evaporation rate is calculated from the date recorded by the laser displacement sensor. The accuracy of the laser displacement sensor is ±10 μm, so the maximum absolute error is 20 μm. During the measurement processes, the minimum depth variation is about 0.2 mm. Therefore, the maximum error of the average evaporation rate is less than 10%. Because of no supplement of the working fluid during the experiment process, the position of the liquid−vapor interface will recede with time, and the maximum receding speed is about 4.3 μm/s. In order to avoid the influence of the receding interface on the measurement of temperature discontinuity, the receding speed of the interface is pre-estimated at a fixed cylinder temperature and pressure ratio, which is considered in each movement of the microthermocouple.

https://dx.doi.org/10.1021/acsomega.1c00134
ACS Omega 2021, 6, 5933−5944

AUTHOR INFORMATION

Corresponding Author

You-Rong Li − *Key Laboratory of Low-Grade Energy Utilization Technologies and Systems of Ministry of Education, School of Energy and Power Engineering, Chongqing University, Chongqing 400044, China;* orcid.org/0000-0001-9489-839X; Email: liyourong@cqu.edu.cn

Authors

Rui-Feng Guo − *Key Laboratory of Low-Grade Energy Utilization Technologies and Systems of Ministry of Education, School of Energy and Power Engineering, Chongqing University, Chongqing 400044, China*

Li Zhang − *Chongqing City Management College, Chongqing 401331, China*

Dong-Ming Mo − *Department of Mechanical Engineering, Chongqing Industry Polytechnic College, Chongqing 401120, China*

Chun-Mei Wu − *Key Laboratory of Low-Grade Energy Utilization Technologies and Systems of Ministry of Education, School of Energy and Power Engineering, Chongqing University, Chongqing 400044, China*

Complete contact information is available at: https://pubs.acs.org/10.1021/acsomega.1c00134

Notes

The authors declare no competing financial interest.

ACKNOWLEDGMENTS

This work is supported by National Natural Science Foundation of China (grant no. 51776022) and Chongqing Basic and Frontier Research Project (no. cstc2019jcyj-msxmX0582).

REFERENCES

(1) Gallego-Elvira, B.; Baille, A.; Martín-Górriz, B.; Martínez-Álvarez, V. Energy balance and evaporation loss of an agricultural reservoir in a semi-arid climate (south-eastern Spain). *Hydrocarbon Process.* **2010**, *24*, 758−766.

(2) Yu, S.; Zhang, Y.; Duan, H. Z.; Liu, Y. M.; Quan, X. J.; Tao, P.; Shang, W.; Wu, J. B.; Song, C. Y.; Deng, T. The impact of surface chemistry on the performance of localized solar-driven evaporation system. *Sci. Rep.* **2015**, *5*, 13600.

(3) Dugas, V.; Broutin, J.; Souteyrand, E. Droplet evaporation study applied to DNA chip manufacturing. *Langmuir* **2005**, *21*, 9130−9136.

(4) Hertz, H. Ueber die Verdunstung der Flüssigkeiten, insbesondere des Quecksilbers, im luftleeren Raume. *Ann. Phys.* **1882**, *253*, 177−193.

(5) Knudsen, M. Die maximale Verdampfungsgeschwindigkeit des Quecksilbers. *Ann. Phys.* **1915**, *352*, 697−708.

(6) Dunn, G. J.; Wilson, S. K.; Duffy, B. R.; David, S.; Sefiane, K. A mathematical model for the evaporation of a thin sessile liquid droplet: comparison between experiment and theory. *Colloids Surf., A* **2008**, *323*, 50−55.

(7) Qin, T.; Tuković, Z.; Grigoriev, R. O. Buoyancy-thermocapillary convection of volatile fluids under atmospheric conditions. *Int. J. Heat Mass Transfer* **2014**, *75*, 284−301.

(8) Kucherov, R. Y.; Rikenglaz, L. E. On hydrodynamic boundary conditions for evaporation and condensation. *J. Exp. Theor. Phys.* **1960**, *10*, 88−89.

(9) Cumin, L. M. G.; Sharipov, F. M.; Kremer, G. M. Rarefied gas flow between two cylinders caused by the evaporation and condensation on their surfaces. *Phys. Fluids* **1998**, *10*, 3203.

(10) Shankar, P. N.; Deshpande, M. D. On the temperature distribution in liquid-vapor phase change between plane liquid surfaces. *Phys. Fluids A* **1990**, *2*, 1030.

(11) Fang, G.; Ward, C. A. Temperature measured close to the interface of an evaporating liquid. *Phys. Rev. E: Stat. Phys., Plasmas, Fluids, Relat. Interdiscip. Top.* **1999**, *59*, 417−428.

(12) Duan, F.; Thompson, I.; Ward, C. A. Statistical-rate-theory determination of water properties below the triple point. *J. Phys. Chem. B* **2008**, *112*, 8605−8613.

(13) Duan, F.; Ward, C. A. Surface excess properties from energy transport measurements during water evaporation. *Phys. Rev. E: Stat. Nonlin. Soft Matter Phys.* **2005**, *72*, 056302.

(14) Popov, S.; Melling, A.; Durst, F.; Ward, C. A. Apparatus for investigation of evaporation at free liquid-vapour interfaces. *Int. J. Heat Mass Transfer* **2005**, *48*, 2299−2309.

(15) Persad, A. H.; Ward, C. A. Statistical rate theory examination of ethanol evaporation. *J. Phys. Chem. B* **2010**, *114*, 6107−6116.

(16) Fang, G.; Ward, C. A. Examination of the statistical rate theory expression for liquid evaporation rates. *Phys. Rev. E: Stat. Phys., Plasmas, Fluids, Relat. Interdiscip. Top.* **1999**, *59*, 441−453.

(17) Ward, C. A.; Fang, G. Expression for predicting liquid evaporation flux: Statistical rate theory approach. *Phys. Rev. E: Stat. Phys., Plasmas, Fluids, Relat. Interdiscip. Top.* **1999**, *59*, 429−440.

(18) Bond, M.; Struchtrup, H. Mean evaporation and condensation coefficients based on energy dependent condensation probability. *Phys. Rev. E: Stat. Nonlin. Soft Matter Phys.* **2004**, *70*, 061605.

(19) Badam, V. K.; Kumar, V.; Durst, F.; Danov, K. Experimental and theoretical investigations on interfacial temperature jumps during evaporation. *Exp. Therm. Fluid Sci.* **2007**, *32*, 276−292.

(20) Kazemi, M. A.; Nobes, D. S.; Elliott, J. A. W. Experimental and Numerical Study of the Evaporation of Water at Low Pressures. *Langmuir* **2017**, *33*, 4578−4591.

(21) Jafari, P.; Masoudi, A.; Irajizad, P.; Nazari, M.; Kashyap, V.; Eslami, B.; Ghasemi, H. Evaporation Mass Flux: A Predictive Model and Experiments. *Langmuir* **2018**, *34*, 11676−11684.

(22) Zhu, Z.-Q.; Liu, Q.-S. Interfacial Temperature Discontinuities in a Thin Liquid Layer during Evaporation. *Microgravity Sci. Technol.* **2013**, *25*, 243−249.

(23) Gatapova, E. Y.; Graur, I. A.; Kabov, O. A.; Aniskin, V. M.; Filipenko, M. A.; Sharipov, F.; Tadrist, L. The temperature jump at water-air interface during evaporation. *Int. J. Heat Mass Transfer* **2017**, *104*, 800−812.

(24) Gatapova, E. Y.; Filipenko, R. A.; Lyulin, I. A.; Marckuk, I. V.; Kabov, O. A. Experimental investigation of the temperature field in the gas-liquid two-layer system. *Thermophys. Aeromech* **2015**, *22*, 701−706.

(25) Hołyst, R.; Litniewski, M. Heat transfer at the nanoscale: evaporation of nanodroplets. *Phys. Rev. Lett.* **2008**, *100*, 055701.

(26) Ward, C. A.; Stanga, D. Interfacial conditions during evaporation or condensation of water. *Phys. Rev. E: Stat. Nonlin. Soft Matter Phys.* **2001**, *64*, 051509.

(27) Ward, C. A.; Duan, F. Turbulent transition of thermocapillary flow induced by water evaporation. *Phys. Rev. E: Stat. Nonlin. Soft Matter Phys.* **2004**, *69*, 056308.

(28) Duan, F.; Badam, V. K.; Durst, F.; Ward, C. A. Thermocapillary transport of energy during water evaporation. *Phys. Rev. E: Stat. Nonlin. Soft Matter Phys.* **2005**, *72*, 056303.

(29) Guo, R.-F.; Zhang, L.; Mo, D.-M.; Wu, C.-M.; Li, Y.-R. Measurement of temperature profile near the evaporating interface in an annular pool with radial temperature gradients at low pressures. *Exp. Therm. Fluid Sci.* **2020**, *119*, 110221.

(30) Kazemi, M. A.; Nobes, D. S.; Elliott, J. A. W. Effect of the Thermocouple on Measuring the Temperature Discontinuity at a Liquid-Vapor Interface. *Langmuir* **2017**, *33*, 7169−7180.

(31) Jafari, P.; Amritkar, A.; Ghasemi, H. Temperature discontinuity at an evaporating water interface. *J. Phys. Chem. C* **2020**, *124*, 1554−1559.

(32) Song, X.; Nobes, D. S. Experimental investigation of evaporation-induced convection in water using laser based measurement techniques. *Exp. Therm. Fluid Sci.* **2011**, *35*, 910−919.
(33) Péraud, J.-P. M.; Landon, C. D.; Hadjiconstantinou, N. G. Monte Carlo methods for solving the Boltzmann transport equation. *Annu. Rev. Heat Transfer* **2014**, *17*, 205−265.

https://dx.doi.org/10.1021/acsomega.1c00134
ACS Omega 2021, 6, 5933−5944